

Transverse NMR Relaxation as a Probe of Mesoscopic Structure

Valerij G. Kiselev^{1,*} and Dmitry S. Novikov²

¹*Section of Medical Physics, University Hospital Freiburg, D79106 Freiburg, Germany*

²*Department of Physics, Massachusetts Institute of Technology, Cambridge, MA 02139*

(Dated: September 24, 2002)

We show that transverse NMR signal relaxation averaged over a macroscopic volume is extremely sensitive to structure of mesoscopic paramagnetic inhomogeneities. Such a sensitivity is proposed as a novel kind of contrast in the NMR measurements. We model the medium by a suspension of arbitrary shaped mesoscopic paramagnetic objects, and find transverse relaxation without adjustable parameters in the case when the dephasing effect of an individual object is small. Results indicate a strong relaxation rate dependence on the shape of the objects. As a major application we consider transverse spin relaxation in the whole blood, for which our theory agrees well with experiments and Monte-Carlo simulations. Applications to a wide range of problems in complex systems (porous media, biological systems, diffusion limited reaction rates) are discussed.

NMR as a structure probe is utilized in the fields as diverse as chemistry, materials science, geology and biomedicine. Pristine specimen found in nature, such as rocks or biological tissues, possess complex structure at a mesoscopic scale. This structure is of primary interest in numerous applications. For example, rock porosity in geology is important to assess the oil basin quality. In biological tissues the mesoscopic scale is set by the size of cells and blood vessels whose properties carry significant diagnostic and physiological information.

It is the NMR monitored *diffusion* that is commonly accepted as a probe of mesoscopic structure in both inorganic [1] and living [2, 3] specimen. In the present Letter we propose a *magnetic susceptibility contrast* as a structure probe. Susceptibility inhomogeneities are often connected to the geometric structure, such as pore walls in porous media. In biological tissues they are brought by paramagnetic cells, such as deoxygenated red blood cells (RBCs) and iron-enriched cells in the brain gray matter. In some cases the susceptibility contrast can be artificially manipulated.

In the present Letter we consider NMR signal from a suspension of arbitrary shaped weakly paramagnetic objects. We demonstrate a significant individual object shape dependence of the transverse relaxation rate. We discuss this result in the biomedical context. Applications of the biomedical NMR imaging (MRI) are limited by a spatial resolution ~ 1 mm, which is larger than the cell size by 2-3 orders of magnitude. Direct resolution enhancement is unfeasible since today MRI hardware hits physiological limits. Our results suggest that further progress can be made by a deeper analysis of the NMR signal since it contains significant information about the paramagnetic tissue structure at the scale of several μm .

We compare our results with experiments on whole blood [4–6], with the objects being paramagnetic RBCs. Previous theoretical efforts in this context were focused on the effect of paramagnetic inclusions of specific geometries (spheres [7, 8] or cylinders simulating blood vessels [7, 9, 10]). The effect of object shape was not studied the-

oretically although experiments [11, 12] and the Monte Carlo simulation [12] indicate a strong shape dependence of the transverse relaxation.

We model the medium by a suspension of $N \gg 1$ identical mesoscopic paramagnetic objects which are randomly placed and oriented. The NMR signal is acquired from nuclear spins that freely diffuse in the solvent and in the objects. A macroscopic volume V of the suspension is characterized by the volume fraction $\zeta = Nv_0/V$ of objects (v_0 = single object's volume). The case of different object species is easily accounted for when $\zeta \ll 1$, since they contribute additively to the relaxation rate [7, 9].

Transverse relaxation occurs due to the two different mechanisms: (i) microscopic spin-spin interactions at the molecular level, (ii) diffusion of spins in the magnetic field induced by mesoscopic objects. Fast processes (i) average out to produce a monoexponential relaxation. Processes (ii) are described in terms of the transverse magnetization density $\psi(\mathbf{r})$, which evolves due to molecular diffusion and spin precession with the local Larmor frequency varying in space. It obeys the Bloch-Torrey equation [13]

$$\frac{\partial \psi}{\partial t} = \left(D \nabla^2 - \frac{1}{T_2} - i\omega_L - i\omega(\mathbf{r}) \right) \psi, \quad (1)$$

where D is the diffusion coefficient of the molecules that carry spins, and T_2 is the relaxation time due to the microscopic interactions. The relaxation rate $1/T_2$ is insensitive to magnetic field inhomogeneities at the mesoscopic scale. Rather, it characterizes local chemical composition. We assume that D and T_2 are the same inside the objects and in the solvent. The constant term ω_L provides the Larmor precession in the homogeneous main field, and $\omega(\mathbf{r}) = \sum_{n=1}^N \omega_0(\mathbf{r} - \mathbf{r}_n)$ is the deviation from ω_L due to the local magnetic fields induced by randomly located paramagnetic objects (as described below).

The signal $S(t)$ from a macroscopic sample is the sum of all spin magnetic moments regardless of their initial positions and their Brownian trajectories after the excitation [9]. In terms of the Green's function $\psi(\mathbf{r}, \mathbf{r}_0, t)$ of (1),

defined by the initial condition $\psi(\mathbf{r}_0, \mathbf{r}, t=0) = \delta(\mathbf{r} - \mathbf{r}_0)$,

$$S(t) = \frac{1}{V} \int d^3\mathbf{r} d^3\mathbf{r}_0 \psi(\mathbf{r}, \mathbf{r}_0, t) \equiv e^{-i\omega_L t - t/T_2} s(t). \quad (2)$$

Microscopic processes decouple due to Eq. (1): $\psi = e^{-i\omega_L t - t/T_2} \phi$, with $\phi(\mathbf{r}, \mathbf{r}_0, t)$ accumulating *mesoscopic* effects. The corresponding signal attenuation factor

$$s(t) = \frac{1}{V} \int d^3\mathbf{r} d^3\mathbf{r}_0 \phi(\mathbf{r}, \mathbf{r}_0, t), \quad s(0) = 1, \quad (3)$$

describing these effects is the main object we focus on.

Consider mesoscopic part $M(\mathbf{r}_0, t) = \int d^3\mathbf{r} \phi(\mathbf{r}_0, \mathbf{r}, t)$ of the spin packet magnetization. The $d^3\mathbf{r}_0$ integration in (3) effectively averages $M(\mathbf{r}_0, t)$ over randomly positioned objects. For $\zeta \ll 1$, M is a product of factors contributed by individual objects [9]. In this case $s(t)$ is expressible in terms of a *single* object dephasing effect $f(t)$ [7, 9]:

$$s = e^{-\zeta f}, \quad f(t) = \left\langle \int \frac{d^3\mathbf{r}_0}{v_0} \left(1 - \int d^3\mathbf{r} \eta(\mathbf{r}_0, \mathbf{r}, t) \right) \right\rangle_o. \quad (4)$$

Here η is the mesoscopic part of the spin packet magnetization density in the presence of a single object,

$$\frac{\partial \eta}{\partial t} = (D \nabla^2 - i\omega_0(\mathbf{r})) \eta, \quad \eta(\mathbf{r}_0, \mathbf{r}, t=0) = \delta(\mathbf{r} - \mathbf{r}_0), \quad (5)$$

and average $\langle \rangle_o$ in (4) is taken over object's orientations.

In the main field $B_0 \hat{\mathbf{z}}$ each paramagnetic object induces a local Larmor frequency shift $\omega_0(\mathbf{r})$ that is determined by the object's *susceptibility profile* $\chi(\mathbf{r})$. Below we use uniformly magnetized objects to compare with experiments: $\chi(\mathbf{r}) = \chi \cdot v(\mathbf{r})$, $\chi \ll 1$, where $v(\mathbf{r})$ is a shape function: $v = 1$ inside and $v = 0$ outside the object. A convolution in \mathbf{r} , ω_0 in the Fourier space is

$$\omega_0(\mathbf{k}) = \delta\omega \cdot Y(\hat{\mathbf{k}}) \cdot \tilde{v}(\mathbf{k}), \quad \delta\omega = 4\pi\chi\omega_L, \quad (6)$$

where $Y(\hat{\mathbf{k}}) = 1/3 - k_z^2/k^2$ is the longitudinal projection of an elementary magnetic dipole field, and the object's form factor $\tilde{v}(\mathbf{k})$ is the Fourier transform of $v(\mathbf{r})$.

Transverse relaxation is qualitatively different in the limits of strong and weak dephasing. Introduce effective object radius ρ as that of a sphere of a volume v_0 . Water molecules pass by the object during the diffusion time

$$t_D = \frac{\rho^2}{D}, \quad \text{where} \quad \frac{4\pi\rho^3}{3} \equiv v_0 = \int d^3\mathbf{r} v(\mathbf{r}). \quad (7)$$

Typical phase acquired by the spins is $\delta\omega \cdot t_D$. In the present work we focus on a weak dephasing case $\delta\omega \cdot t_D \ll 1$ (diffusion narrowing regime). This regime covers a variety of experiments, in particular spin dephasing in diamagnetic and paramagnetic samples in the field $B_0 \lesssim 1$ Tesla.

We find the Green's function η of Eq. (5) perturbatively in the small parameter $\delta\omega \cdot t_D$, and use Eq. (4)

to obtain $f(t)$. This approach is analogous to the Born series for the quantum mechanical scattering amplitude.

The zeroth order in $\delta\omega \cdot t_D$ describes free diffusion. In this case the total magnetization of each spin packet is conserved, $\int d^3\mathbf{r} \eta(\mathbf{r}_0, \mathbf{r}; t) = 1$ in (4), and $s(t) = 1$. The first order correction to f vanishes since it is proportional to the angular average of the dipole field. The expression for f is dominated by the second order in $\delta\omega \cdot t_D$ (Fig. 1):

$$f(\tau) = \frac{2\pi\alpha^2}{15} \int_0^\infty \frac{dq}{q^2} g(q^2\tau) \int \frac{d\hat{\mathbf{q}}}{4\pi} \left| \frac{\tilde{v}(\mathbf{q})}{\tilde{v}(\mathbf{0})} \right|^2, \quad (8)$$

$$\alpha \equiv \frac{2}{3\pi} \delta\omega \cdot t_D. \quad (9)$$

Here τ is the dimensionless time $\tau = t/t_D$. The inner integral in Eq. (8), which is taken over the directions of $\mathbf{q} = \mathbf{k}\rho$, depends exclusively on the object shape. The object size enters Eq. (8) only through the diffusion time t_D , Eq. (7). The function g depends on the particular sequence of the radiofrequency (rf) pulses applied to manipulate the spins and will be discussed below.

As a conservative estimate, the formal series for $f(t)$ converges when $\alpha < 1$. Indeed, each successive term in the perturbative expansion of $f(t)$ is multiplied by the dimensionless factor $i\alpha = i4\pi/(2\pi)^3 (\delta\omega \cdot t_D) (v_0/\rho^3)$. Angular integrations of the products $Y(\hat{\mathbf{k}}_1)Y(\hat{\mathbf{k}}_2)\dots$ improve convergence by bringing additional factors < 1 that are object shape specific and hard to account for in general.

Odd orders of the expansion in α are imaginary. They renormalize the homogeneous component of the suspension's magnetic susceptibility. Since the first order vanishes the correction to ω_L is proportional to α^3 . The signal attenuation is determined by the even orders in α . The correction to (8) is of the order of α^4 and is negative.

Consider the free induction decay (FID), an evolution after a single rf $\pi/2$ pulse which creates the maximal transverse spin magnetization. The function g in (8), denoted as g_{FID} , is proportional to a time convolution of the three free diffusion propagators $\eta^{(0)}(\mathbf{q}, \tau) = \theta(\tau)e^{-q^2\tau}$, $\theta(\tau)$ being a unit step function (Fig. 1, left):

$$g_{\text{FID}}(q^2\tau) = q^2\tau - 1 + e^{-q^2\tau}. \quad (10)$$

To reduce sensitivity to large scale field inhomogeneities, samples are often irradiated by a number of refocusing rf π -pulses. Each such pulse quickly rotates the spins by π around an axis which is transverse to $\hat{\mathbf{z}}$. This is equivalent to a complex conjugation of η developed up until this time moment. The resulted distribution η^* is the initial condition for the further evolution.

In the spin echo (SE) technique [14] a single π -pulse is applied at the time $t_E/2$ and the signal is measured at $t = t_E$. The corresponding g -function reads

$$g_{\text{SE}} = q^2\tau_E - 3 + 4e^{-q^2\tau_E/2} - e^{-q^2\tau_E}, \quad \tau_E = \frac{t_E}{t_D}. \quad (11)$$

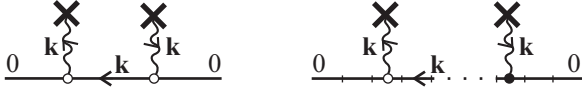


FIG. 1: Second order processes for $f(t)$. *Left*: FID relaxation. Circles, wavy lines and crosses stand for $-i\delta\omega$, $Y(\mathbf{k})$ and $\tilde{v}(\mathbf{k})$ respectively. Solid lines represent free propagators $\eta^{(0)}(\mathbf{k}, \tau)$ in time intervals between interactions. External momenta are set to zero due to Eq. (3). *Right*: CPMG relaxation. Each section represents a free propagator $\eta^{(0)}$ in the interval Δt between successive refocusing pulses. Complex conjugation on every other interval Δt is indicated with the filled circle. Eq. (12) is obtained as a sum of all such configurations.

In the CPMG protocol [15] refocusing π -pulses are generated in a long train and the steady state signal is studied as a function of the interpulse interval Δt (Fig. 1, right):

$$g_{\text{CPMG}} = q^2\tau - 2 \tanh \frac{q^2\tau}{2}, \quad \tau = \frac{\Delta t}{t_D}. \quad (12)$$

Eqs. (10, 11, 12) yield that at $\tau \ll 1$, $f \propto \tau^2$ for the FID and $f \propto \tau^3$ for the SE and the CPMG sequences. Asymptotic expansion of (8) in $\tau^{-1/2}$ at $\tau \gg 1$ gives

$$r_2 \equiv \frac{f(\tau)}{\tau} \simeq \frac{2\pi\alpha^2}{15} \left(\int_0^\infty dq \int \frac{d\hat{\mathbf{q}}}{4\pi} \left| \frac{\tilde{v}(\mathbf{q})}{\tilde{v}(\mathbf{0})} \right|^2 - \frac{A}{\sqrt{\tau}} \right), \quad (13)$$

with $A_{\text{FID}} = \sqrt{\pi}$, $A_{\text{SE}} = (2\sqrt{2} - 1)\sqrt{\pi}$, and $A_{\text{CPMG}} = (2\sqrt{2} - 1)\zeta(3/2)/\sqrt{\pi} \approx 2.695$ for the considered pulse sequences. The dimensionless NMR relaxivity r_2 is shown in Fig. 2, left, for the case of the homogeneously magnetized spherical particles. Shape dependence is illustrated in Fig. 2, right for the case of disk-shaped objects. The height-to-radius ratio c defines the disk shape, with $c = 0.5$ being close to the intact RBC.

Below we analyze our results given by Eqs. (8, 13).

(i) *Relaxation (4) is non-monoexponential with f crucially depending on the object shape.* It is the form factor $\tilde{v}(\mathbf{k})$ that governs the convergence of the integral for large $\mathbf{q} = \mathbf{k}\rho$ in (8). The integral converges at $k \sim 1/\rho$, allowing one to probe the object's structure. (A direct quantum mechanical analogy is scattering amplitude dependence on the form factor of the external potential.) A point-like magnetization $v \propto \delta(\mathbf{r})$ causes a divergence in Eqs. (8, 13). In the present case this “nonrenormalizability” (non-universal cutoff dependence) effectively increases sensitivity in the NMR measurements.

(ii) *Shape sensitivity is a consequence of a singular interaction $Y \sim r^{-s}$ between nuclear spins and objects.* Consider the case when the singularity in Y is cut off at a scale $r < a$. Then $Y(\mathbf{k}) \rightarrow 0$ as $ka > 1$. If $a > R$, the integral in Eq. (8) is insensitive to the form factor since it converges at $k < 1/a < 1/R$, destroying shape sensitivity. Physically, such a cutoff introduces a spherical “cloud” of a radius a around each object. This cloud smears information about the object's structure. The power necessary for shape dependence is $s > 2 + (d - 2)/N$ for the

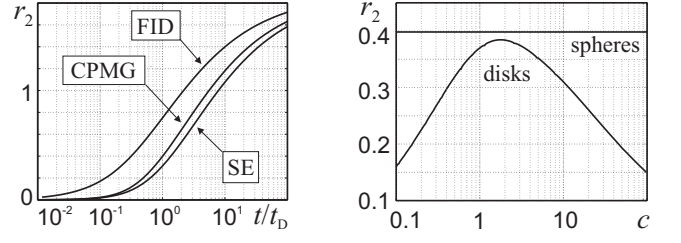


FIG. 2: Mesoscopic relaxivity $r_2 = t_D/(\zeta T_2^*) \equiv f(\tau)/\tau$ for $\alpha^2 = 15/2\pi$. *Left*: Objects are spheres, $t = t_E$ for the SE, $t = \Delta t$ for the CPMG. *Right*: Shape effect: disks vs. spheres. CPMG relaxivity $r_2(\Delta t/t_D = 1)$, objects are disks with height-to-radius ratio c , and spheres of the same volume.

N -th order in d dimensions. Thus both magnetic dipole ($s = 3$) and contact interaction $Y = \delta(\mathbf{r})$ in $d = 3$ yield shape sensitivity already in the second order, as shown above. On the other hand, e.g. a $1/r$ singularity in Y is not enough to probe the structure of the objects.

(iii) *Shape sensitivity is present for any field B_0 .* Above we demonstrated shape sensitivity in the domain where perturbative approach is reliable ($\alpha \ll 1$). We now prove it for any α . Integrals like (8) whose convergence is form factor dependent appear in each order of the perturbation series for $f(t)$. Although angular integrations impede explicit summation of this series, they do not cause non-analyticity at $\alpha = 0$, and thus radius of convergence in $\alpha \propto B_0$ is finite. Therefore the series can be analytically continued to the large field domain $\alpha > 1$ where the perturbation theory formally breaks up. The final result for $f(t)$ would still be form factor dependent, which proves shape sensitivity for *any* field.

(iv) *Shape sensitivity is not limited by NMR physics.* Consider a *chemical reaction rate* in the presence of a diffusion limited absorption on impurities. The rate equation is obtained from (1) by analytical continuation $-i\omega_L, -i\omega(\mathbf{r}) \rightarrow u_0, u(\mathbf{r})$, where u_0 is the background reaction rate, and Eq. (6) with $Y(\mathbf{k}) = 1$ yields its impurity density induced local deviation $u(\mathbf{r}) = \delta u \cdot v(\mathbf{r})$. The (nonzero) first order term gives the object's integrated absorption rate. The second order (8) with g_{FID} yields impurity *density profile* correction to the rate with $-\frac{2}{3\pi}(\delta u \cdot t_D)^2$ in front of the integral.

Below we compare the results (8, 13) with experiments. As a first test we use the reported relaxation rate in dilute ($\zeta = 0.02$) suspensions of polystyrene microspheres in paramagnetically doped water [16] (Fig. 3, left).

Further experiments were performed on the deoxygenated blood with a high RBC volume fraction $\zeta = 0.40 - 0.60$ [4–6]. To apply Eqs. (8, 13) one needs to take into account a slower diffusion inside the cells and to extend our approach for large ζ . The former will be considered elsewhere. For now, we obtain upper and lower estimates for the relaxation rate by using in Eq. (8) the values $D_{\text{in}}, D_{\text{out}}$ of the diffusion coefficient in erythro-

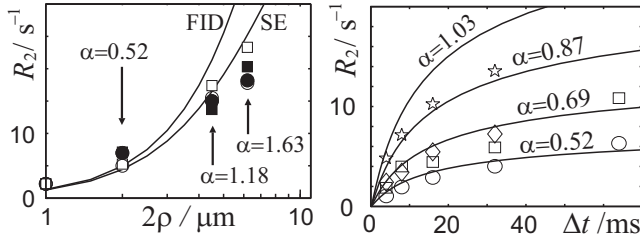


FIG. 3: Theory (lines) vs. experiments (symbols). *Left*: Relaxation rate $R_2 = -(\ln s)/t$ for the FID (boxes) and SE (circles) as a function of the particle diameter. Filled and hollow symbols correspond to measured and Monte Carlo simulated relaxation rates [16]. *Right*: CPMG relaxation rate for the human blood samples [6] for $B_0 = 1.41, 1.18, 0.94, 0.71$ T (from top to bottom). Experimental errors are 10–20% [6]. Following our discussion after Eq. (8), theory agrees with experiment for small α and overestimates it for $\alpha \simeq 1$.

cytes and plasma respectively.

The $\zeta \sim 1$ case poses a challenging task equivalent to finding the statistical sum of a dense gas of objects. Instead we replace ζ by $\zeta(1 - \zeta)$ in (4), which is well supported experimentally [17]. Such a replacement is justified by the virial expansion. Eq. (4) treats exactly the first cumulant of the statistical sum. The second cumulant provides an $\mathcal{O}(\zeta^2)$ *negative* correction. This together with vanishing mesoscopic contribution as $\zeta \rightarrow 1$ justifies a quadratic polynomial interpolation, $\zeta(1 - \zeta)$. The latter is correct as $\zeta \rightarrow 0$ and 1, and describes a crossover between the dilute and the extremely dense cases.

The relaxation rate in deoxygenated blood measured in [4] quadratically depends on the magnetic field, $-(\ln s)/t = \kappa_1 B_0^2$, in agreement with Eq. (8). The proportionality coefficient κ_1 was found to be $7.2 s^{-1} T^{-2}$ for the CPMG pulse sequence with $\Delta t = 4$ ms. In [4], the field range $B_0 = 0.05 - 1.5$ T yields $\alpha = 0.033 - 0.99$. We calculated $\zeta = 0.55$ from the parameters given in [4], utilized the magnetic susceptibility of the deoxygenated RBCs $\chi = 2.7 \times 10^{-7}$ [5], and simulated the intact erythrocytes by disks of the known volume of $87 \mu m^3$ with the height-to-radius ratio of $c = 0.5$. Using $D_{out} = 2.20 \mu m^2/ms$ and $D_{in} = 0.76 \mu m^2/ms$ [18], our theory gives $4.7 < \kappa_{1th} < 5.6 s^{-1} T^{-2}$.

To assess this result we note that neither the susceptibility of RBCs nor their actual shape were reported in [4]. Chemicals used to treat the samples are likely to change osmotic pressure in plasma, which would deform the RBCs thus changing all relevant parameters.

Quadratic dependence of the SE blood relaxation rate on χ , which follows from Eq. (8), was confirmed by varying the RBC oxygen saturation y in the field $B_0 = 1.5$ T [5]: $-(\ln s)/t = \kappa_2(0.95 - y)^2$, with the measured coefficient $\kappa_2 = 55 s^{-1}$ for $\zeta = 0.3$ and $\kappa_2 = 59 s^{-1}$ for $\zeta = 0.4$. Our approach results in the corresponding ranges $26 < \kappa_{2th} < 56 s^{-1}$ and $30 < \kappa_{2th} < 64 s^{-1}$.

The CPMG relaxation rate $R_2 = -(\ln s)/t$ in the

whole blood was measured [6] as a function of the interecho interval (Fig 3, right) for $0.71 < B_0 < 1.41$ T. We simulated blood as described above using $D = D_{out}$ for plasma. The use of the value D_{in} instead of D_{out} yields about the same rate R_2 for the short times and approximately a two-fold increase of R_2 for the large times.

This brief survey shows that, although crude, our model captures essential features of the NMR relaxation. Experiments at higher fields of 2.35 T [11] and 4.7 T [12] have both $\alpha > 1$ and $\zeta \sim 1$, hence we achieve only qualitative agreement with the measured relaxation curves. Quantitative agreement can be easily reached [8] using t_D and α as fitting parameters or by fitting to a simple chemical exchange model [19]. However, fitting has a predictive power when the signal universally depends on a handful of phenomenological parameters. Shape sensitivity makes such a fitting meaningless in the case of varying tissue structure. Due to the same reason, in experiments analogous to [4–6, 11, 12] it is essential to control volume fraction, shape and susceptibility of paramagnetic objects, and effective diffusion coefficient in the sample.

To conclude, presented theory of transverse relaxation in suspensions of mesoscopic paramagnetic objects yields object shape sensitivity as a novel type of contrast in NMR measurements. Theory agrees with experiments in a predicted range and points at a set of parameters essential to control in experiments on complex samples.

D.N. appreciates a visiting grant and hospitality of the Section of Medical Physics, University Hospital Freiburg.

* Electronic address: kiselev@ukl.uni-freiburg.de

- [1] P.P. Mitra *et al.*, Phys. Rev. Lett. **68**, 3555 (1992)
- [2] Le Bihan D, ed., *Diffusion and Perfusion Magnetic Resonance Imaging*, Raven Press, 1995
- [3] D.A. Yablonskiy *et al.*, PNAS **99** 3111 (2002)
- [4] R.A. Brooks *et al.*, J. Mag. Res. Imag. **4**, 446 (1995)
- [5] W.M. Spees *et al.*, Mag. Res. Med. **45**, 533 (2001)
- [6] J.M. Gomori *et al.*, J. of Computer Assisted Tomography **11**, 684 (1987)
- [7] D.A. Yablonskiy and E.M. Haacke, Mag. Res. Med. **32**, 749 (1994)
- [8] J.H. Jensen, R. Chandra, Mag. Res. Med. **44**, 144 (2000)
- [9] V.G. Kiselev and S. Posse, Phys. Rev. Lett. **81**, 5696 (1998), **83**, 1487 (1999); Mag. Res. Med. **41**, 499 (1999)
- [10] W.R. Bauer *et al.*, Phys. Rev. Lett. **83**, 4215 (1999)
- [11] F.Q. Ye and S. Allen, Mag. Res. Med. **34**, 713 (1995)
- [12] P. Gillis *et al.*, Mag. Res. Med. **33**, 93 (1995)
- [13] H.C. Torrey, Phys. Rev. **104**, 563 (1956)
- [14] E.L. Hahn, Phys. Rev. **80**, 580 (1950)
- [15] H.Y. Carr and E.M. Purcell, Phys. Rev. **94**, 630 (1954); S. Meiboom and D. Gill, Rev. Sci. Instr. **29**, 688 (1959)
- [16] R. Weisskoff *et al.*, Mag. Res. Med. **31**, 601 (1994)
- [17] K.R. Thulborn *et al.*, Biochim. Biophys. Acta **714** (2): 265 (1982)
- [18] J.G. Li *et al.*, Mag. Res. Med. **40**, 79 (1998)
- [19] R.A. Brooks *et al.*, Mag. Res. Med. **45**, 1014 (2001).